Atmospheric Environment 254 (2021) 118383

Contents lists available at ScienceDirect

Atmospheric Environment

journal homepage: http://www.elsevier.com/locate/atmosenv

Short communication

On the photolysis branching ratio of methyl ethyl ketone

Anna G. Zborowska, Ceara Y. MacInnis, Connie Z. Ye, Hans D. Osthoff *

Department of Chemistry, 2500 University Drive NW, University of Calgary, Calgary, AB T2N 1N4, Canada

GRAPHICAL ABSTRACT

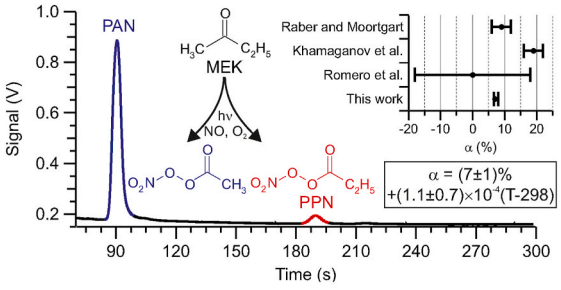

ARTICLE INFO

Keywords:
Methyl ethyl ketone (MEK)
Photolysis branching ratio
End product study
Master chemical mechanism (MCM)

ABSTRACT

The methyl ethyl ketone (MEK) photolysis branching ratio (α) was re-evaluated by an end product analysis and box model simulations with the Master Chemical Mechanism (MCM). Using light emitting diodes centered at 285 nm or 315 nm, MEK was irradiated in the presence of nitric oxide and oxygen to produce peroxyacetic and peroxypropanoic nitric anhydride, $CH_3C(O)O_2NO_2$ (PAN) and $C_2H_5C(O)O_2NO_2$ (PPN), which were quantified by gas chromatography. Box model simulations indicated that PPN is partially produced as a secondary product from chemistry initiated by reaction of the hydroxyl radical (OH) with MEK. Under NO_x-limited experimental conditions or in the presence of ethane as an OH quencher, the product distribution observed required $\alpha = (7 \pm 1)\% + (1.1 \pm 0.7) \times 10^{-4} \times (T-298)$ for $250K < T < 300K$ (2σ uncertainty), independent of pressure (at pressures > 266 hPa) and consistent with current IUPAC recommendations.

1. Introduction

The trace gas methyl ethyl ketone (MEK; 2-butanone; $CH_3C(O)C_2H_5$) is an important constituent of the troposphere (Yáñez-Serrano et al., 2016) and the second-most abundant atmospheric ketone after acetone (Brewer et al., 2019). Its concentrations are elevated in biomass burning plumes (Hornbrook et al., 2011), industrial emissions (Legreid et al., 2007), and automobile exhaust (Kean et al., 2001). It is also produced photochemically, e.g., from photo-oxidation of n-butane and 3-methylpentane (Sommariva et al., 2011) and on the ocean surface (Brewer et al., 2020). The main atmospheric fate of MEK is oxidation by the hydroxyl radical (OH) (Wallington and Kurylo, 1987) and photolysis (Pitts and Blacet, 1950) via the following pathways:

$$C_2H_5C(O)CH_3 + h\nu \rightarrow CH_3C(O) + C_2H_5 \ (\lambda < 342 \text{ nm}) \quad \text{(R1a)}$$

$$C_2H_5C(O)CH_3 + h\nu \rightarrow C_2H_5C(O) + CH_3 \ (\lambda < 339 \text{ nm}) \quad \text{(R1b)}$$

$$C_2H_5C(O)CH_3 + h\nu \rightarrow C_2H_5 + CO + CH_3 \ (\lambda < 303 \text{ nm}) \quad \text{(R1c)}$$

* Corresponding author.
E-mail address: hosthoff@ucalgary.ca (H.D. Osthoff).

https://doi.org/10.1016/j.atmosenv.2021.118383
Received 3 June 2020; Received in revised form 26 March 2021; Accepted 28 March 2021
Available online 1 April 2021

Photolysis dominates over loss to OH in the troposphere, especially at higher elevations (Brewer et al., 2019).

While the absorption cross-sections (Brewer et al., 2019; Martinez et al., 1992; Yujing and Mellouki, 2000), dissociation thresholds (Atkinson et al., 2006) and dynamics (Diau et al., 2001; Sølling et al., 2002), and overall quantum yields (Nádasdi et al., 2010; Rajakumar et al., 2008), including their pressure dependence (Raber and Moortgat, 1995), are known, the photolysis product distribution is less certain, though it is clear that under tropospheric conditions pathway R1a is dominant, and R1c is negligible. The branching ratio currently recommended by the atmospheric chemical kinetic data evaluation task group of the International Union of Pure and Applied Chemistry (IUPAC) (Atkinson et al., 2006),

$$\alpha = k_{1b}/(k_{1a}+k_{1b}) \quad (1)$$

is based on the study by Raber and Moortgart (1995) who analyzed the photoproducts following broadband irradiation (280 nm–340 nm) of MEK. They converted the acyl radicals produced by R1a and R1b with O_2 to peroxyacetyl (PA) and peroxypropionyl (PP) radicals, which were further reacted with nitrogen dioxide (NO_2) to peroxyacetic and peroxypropanoic nitric anhydride (PAN and PPN) (Raber and Moortgat, 1995).

$$CH_3C(O) + O_2 + M \rightarrow CH_3C(O)O_2\,(PA) + M \quad (R2a)$$

$$C_2H_5C(O) + O_2 + M \rightarrow C_2H_5C(O)O_2\,(PP) + M \quad (R3a)$$

$$CH_3C(O)O_2 + NO_2 \rightleftharpoons CH_3C(O)O_2NO_2\,(PAN) \quad (R4)$$

$$C_2H_5C(O)O_2 + NO_2 \rightleftharpoons C_2H_5C(O)O_2NO_2\,(PPN) \quad (R5)$$

Though detection of PPN was "not quantitative" (Raber and Moortgat, 1995), box model simulations showed that R1a accounted for 80%–90% and R1b for 5%–10% of the total MEK photolysis reaction (Raber and Moortgat, 1995), which put α in the range of 0.06–0.12. Follow-up studies, however, have yielded mixed results. For example, Khamaganov et al. (2007) monitored the methyl radical (CH_3) via its absorption at 216.4 nm produced during MEK photolysis at 248 nm and deduced a branching ratio of $\alpha = 0.19 \pm 0.03$. Romero et al. (2005a; 2005b) also irradiated MEK with a 248 nm laser, but monitored the OH produced in minor channels in the reactions of $CH_3C(O)$ and $C_2H_5C(O)$ with O_2:

$$CH_3C(O) + O_2 \rightarrow OH + \text{products} \quad (R2b)$$

$$C_2H_5C(O) + O_2 \rightarrow OH + \text{products} \quad (R3b)$$

The reactions between the acyl radicals with O_2 initially yield "energized" reaction intermediates, $CH_3C(O)O_2^*$ and $C_2H_5C(O)O_2^*$, which either produce OH via pressure-independent channels (R2b and R3b) or collide with the base gas and produce PA and PP (R2a and R3a) (Papadimitriou et al., 2015). Because of this competition, observed OH yields are functions of pressure. Moreover, they are sufficiently different, allowing relative abundances of the corresponding acyl radicals to be determined. Romero et al. (2005a) deduced a branching ratio of $\alpha = 0.00 \pm 0.18$ from the observed pressure dependence of the OH production rates. Even though considerably lower OH yields have since been reported for R2b and R3b (Papadimitriou et al., 2015; Zügner et al., 2010), a branching ratio of $\alpha = 0$ was implemented for MEK photolysis in the Master Chemical Mechanism (MCM), a near-explicit chemical mechanism of the degradation of volatile organic compounds to assess ground-level ozone (O_3) formation (Jenkin et al., 1997, 2012; Saunders et al., 2003). Although it is known that the MEK absorption cross-section increases with temperature (Brewer et al., 2019; Nádasdi et al., 2010) and that the overall quantum yields (Nádasdi et al., 2010) and OH production rates (Romero et al., 2005a, 2005b) are pressure-dependent, the value and temperature and pressure dependence of α are not well constrained by experiment.

In a recent air quality study in the Uintah basin in which the MCM was utilized to model O_3 formation, it was found that oxygenated volatile organic compounds (VOCs), such as MEK, constituted an important source of radicals during wintertime O_3 pollution events (Edwards et al., 2013, 2014). While the model was able to reproduce O_3 and MEK abundances, ratios of PPN to PAN were larger than predicted, 0.20:1 compared to 0.12:1 (Edwards et al., 2014). The choice of $\alpha = 0$ for MEK and other asymmetrically substituted ketones in the MCM may have contributed to this discrepancy, as $\alpha > 0$ would have yielded a higher PPN:PAN ratio. This ratio is often used to assess the contribution of anthropogenic VOCs to photochemical O_3 formation (Roberts et al., 1998; Zhang et al., 2015).

Our laboratory has built a gas chromatograph for quantification of peroxycarboxylic nitric anhydrides (PAN-GC) such as PAN and PPN (Tokarek et al., 2014) and a photochemical source (Furgeson et al., 2011; Rider et al., 2015) in which PAN or PPN are generated from photolysis of acetone or 3-pentanone in the presence of O_2 and a calibrated amount of either nitric oxide (NO) or NO_2; NO may be used as it is oxidized to NO_2 by peroxy radicals.

In this work, we used the PAN-GC and photochemical source to determine the PPN:PAN ratio generated during MEK photolysis in the presence of NO and O_2 as functions of temperature and pressure. The majority of the experiments were conducted with light-emitting diodes (LEDs) at 285 nm, where the MEK absorption cross-section and photoproduct yields are largest. The experimental work was complimented by MCM box model calculations. Additional experiments were conducted at 315 nm to probe the potential wavelength dependence (Pitts and Blacet, 1950) and atmospheric relevance of R1 and in the presence of ethane to assess the potential impact of secondary OH chemistry.

2. Experimental

2.1. Experiments with 285 nm LEDs

The sample gas streams were generated by flowing O_2 (Praxair) through a 3-neck glass trap (Furgeson et al., 2011) containing several mL of liquid MEK (Sigma-Aldrich, ACS reagent grade >99%, used as received) at a flow rate of 20 standard cubic centimeters per minute (sccm) set using a mass flow controller (MFC, Celerity) and combined with 2 sccm of 1.96 parts-per-million (by volume; ppmv) dry NO in N_2 (Scott-Marrin) delivered using an all-metal MFC (MKS). Under these conditions, PAN and PPN production was limited by the amount of NO added, as judged from high ratios of ΣPAN to NO_2 observed by thermal dissociation cavity ring-down spectroscopy in earlier experiments (Rider et al., 2015). The internal components of the photochemical PAN source were remounted to enable temperature and pressure monitoring and control. Gas mixtures were irradiated in a cylindrical quartz reaction chamber (length 22.3 cm, outer diameter 4.9 cm, volume 450.5 cm^3) by three ultraviolet (UV-) LEDs (Thorlabs LED285W) that have a center wavelength of 285 ± 5 nm, a full-width at half-maximum of 12 nm, and combined optical power of 2.4 mW (Rider et al., 2015). This wavelength region was chosen because of its overlap with the $n \rightarrow \pi^*$ absorption band of MEK (Brewer et al., 2019). The cylinder was submerged in a refrigerated circulating bath (VWR) containing an ethylene glycol/water mixture and pressure-controlled using a MKS 640A pressure controller connected to a vacuum pump. All connecting tubing was constructed from 0.635 cm outer and 0.476 cm inner diameter Teflon™ tubing and fittings.

The Varian PAN-GC with electron capture detector (ECD) described by Tokarek et al. (2014) was used for quantification of PAN and PPN. Part of the gas mixture emerging from the cylinder was drawn through a polyether ether ketone (PEEK) sample loop (0.02 mL internal volume) whose content were injected onto the GC column every 5 min. The relative sensitivity of PPN:PAN was 0.96 ± 0.04 (Tokarek et al., 2014).

2.2. Box model simulations

Box model simulations were carried out to assess the extent by which the product distribution may be shifted by secondary chemistry. A reaction subset generated from the MCM (V3.3.1) for MEK and $C_2H_5CO_3$ was obtained via http://mcm.leeds.ac.uk/MCM (Jenkin et al., 1997, 2012; Saunders et al., 2003) and run using the Atchem V1.5 online tool (Sommariva et al., 2020). Reaction R1b was added to this mechanism with yield α and the rate coefficient of reaction R1a was scaled by (1-α). The PAN and PPN thermal decomposition rates were updated to those of Kabir et al. (2014) with T in Kelvin:

$$PAN \rightarrow CH_3C(O)O_2 + NO_2,\ k_{-4} = 2.83 \times 10^{16} e^{-13592/T}\ cm^3\ molec.^{-1}\ s^{-1} \quad (R\text{-}4)$$

$$PPN \rightarrow C_2H_5C(O)O_2 + NO_2,\ k_{-5} = 2.36 \times 10^{16} e^{-13592/T}\ cm^3\ molec.^{-1}\ s^{-1} \quad (R\text{-}5)$$

The general approach adopted in the MCM is that each peroxy radical is assumed to react with all other peroxy radicals (i.e., the peroxy radical "pool") at a single, collective rate (Jenkin et al., 1997). In the mechanism extracted from the MCM web site, the rate coefficients for the reactions of $CH_3C(O)O_2$ with RO_2 were about ½ those of the reactions of $C_2H_5C(O)O_2$ with RO_2, at odds with experiment (Le Crâne et al., 2005; Villenave et al., 1998) and MCM documentation. Following a personal communication with Andrew Rickard and Mike Jenkin, the rate coefficients for $CH_3C(O)O_2$+RO_2 were changed to those for $C_2H_5C(O)O_2$+RO_2:

$$CH_3C(O)O_2 + RO_2 \rightarrow CH_3C(O)O_2H,\ k_{6a} = 3.0 \times 10^{-12}\ cm^3\ molec.^{-1}\ s^{-1} \quad (R6a)$$

$$CH_3C(O)O_2 + RO_2 \rightarrow CH_3O_2 + CO_2,\ k_{6b} = 7.0 \times 10^{-12}\ cm^3\ molec.^{-1}\ s^{-1} \quad (R6b)$$

Photolysis frequencies were calculated by multiplying absorption cross-sections and quantum yields from the NASA-JPL evaluation (Burkholder et al., 2015) with the spectrum of the UV-LEDs (Rider et al., 2015) and modulated in time using a trapezoidal function to simulate the gas mixture passing through the photolysis cell.

2.3. Comparison of PPN:PAN ratios obtained at 285 nm with 315 nm

A wavelength of 285 nm is just below the wavelength cut-off of the actinic flux in the troposphere. To probe if the results obtained at 285 nm are applicable to tropospheric conditions, a second set of experiments was conducted in which an array of three UV-LEDs emitting at 315 nm center wavelength (Thorlabs LED315W) was exchanged with the 285 nm LEDs. Since the NO cylinder used for the experiments described in the preceding section had run empty and an equivalent replacement was not on hand, the procedure to generate gas mixtures was modified as follows: A gas stream of O_2 was flown at 6 sccm past a permeation tube filled with MEK heated to 70 °C and combined with 0.2 sccm of 100.2 ppm NO in N_2 (Scott-Marrin) prior to photolysis at ambient pressure and temperature. The product ratios were analyzed with the Hewlett Packard (HP) 5890 PAN-GC described by Rider et al. (2015). The PPN peak areas were scaled by a factor of 1/0.964 to account for the lower PPN sensitivity.

2.4. OH quenching experiment

A third set of experiments was conducted at 285 nm to verify the extent by which the PPN:PAN ratios are affected by OH-initiated chemistry. Ethane (C_2H_6) was added as an OH quencher for half of these experiments. MEK was delivered from a 3-neck glass trap with either 20 sccm of O_2 or 14.6 sccm of O_2 (in which case 5.4 sccm of C_2H_6 were added downstream). This was then combined with 0.2 sccm of NO from the 100.2 ppm NO in N_2 cylinder. Photolysis was carried out at room temperature and atmospheric pressure. The PPN:PAN ratios were determined using the HP 5890 PAN-GC, set to automatically inject every 5 min. Experiments were run over a period of several days, both in the absence and in the presence of C_2H_6.

3. Results and discussion

3.1. PPN:PAN ratios obtained with 285 nm radiation

Ratios of PPN:PAN obtained from MEK irradiation at 285 nm in the presence of NO and O_2 ranged from 5.9% to 8.1%. Shown in Fig. 1 are PPN:PAN ratios obtained from irradiation at 298 K, binned by pressure. A pressure-independent product ratio of (7.2 ± 0.2)% was observed from ~260 to ~690 hPa (~200 to ~525 Torr).

The temperature dependence of the PPN:PAN ratio was investigated at a pressure of 330 hPa (250 Torr; Fig. 2). The PPN:PAN ratio increases with temperature with a slope of $(1.1 \pm 0.4) \times 10^{-4}\ K^{-1}$. An Arrhenius plot analysis gives an activation barrier of (0.9 ± 0.3) kJ mol^{-1} for the less favorable reaction (R1b).

3.2. Box model simulations

To investigate how secondary chemistry may shift the product distribution, MCM simulations were carried out at five temperatures (from 253 K to 293 K) and 330 hPa (250 Torr). The first simulation (Fig. 3, green trace) was carried out using the MCM default value, α = 0. The simulation predicts a PPN:PAN ratio of ~0.8%. In this case, the PPN stems from reaction of OH with MEK to form the ethoxymethylperoxy radical:

$$MEK + OH\ (+O_2) \rightarrow C_2H_5C(O)CH_2O_2 \quad (R7)$$

This radical reacts with NO, the hydroperoxyl radical (HO_2), or other RO_2 to form the alkoxy radical $C_2H_5C(O)CH_2O$ (with minor paths leading to ethyl glyoxal and $C_2H_5C(O)CH_2O_2H$), all of which yield the PP radical, $C_2H_5C(O)O_2$, which in turn reacts with NO_2 to PPN via (R5).

Next, α was parameterized using the intercept from Fig. 1 and the slope from Fig. 2, i.e., $\alpha = 0.072 + 1.06 \times 10^{-4} \times (T\text{-}298)$. The model results are shown as a red trace in Fig. 3 and overestimate the observations by 0.7%, which is nearly identical to what was produced by secondary chemistry in the α = 0 case (Fig. 3, green trace). Subtracting this offset from the parameterization gives $\alpha = 0.065 + 1.06 \times 10^{-4} \times (T\text{-}298)$, with which a final simulation set was run (Fig. 3, purple trace). This simulation reproduced the observations.

3.3. PPN:PAN ratios obtained with 315 nm radiation

To probe the atmospheric relevance of the results at 285 nm, PPN:PAN peak area ratios observed with 315 nm UV-LEDs were compared

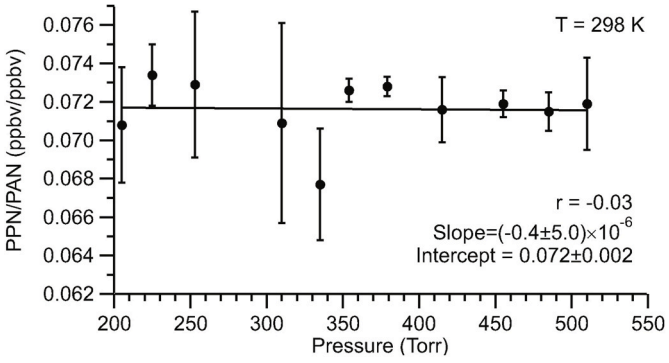

Fig. 1. Observed PPN:PAN ratios upon irradiation of MEK at 285 nm in the presence of NO and O_2 at 298 K as a function of pressure. Each data point is an average of between 4 and 19 chromatograms. The error bars indicate ±1 standard deviation (σ), i.e., measurement precision.

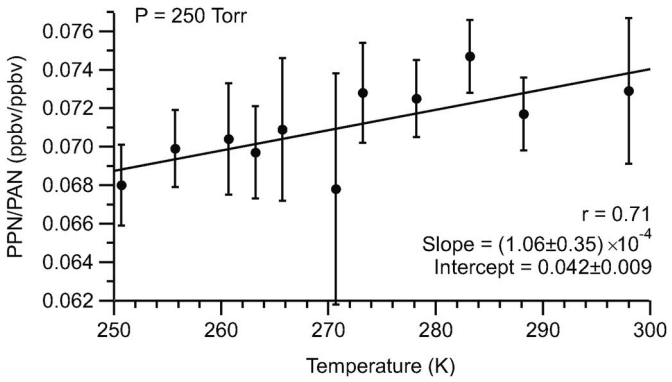

Fig. 2. PPN:PAN ratios from irradiation of MEK at 285 nm in the presence of NO and O_2 as a function of temperature at a pressure of 250 Torr.

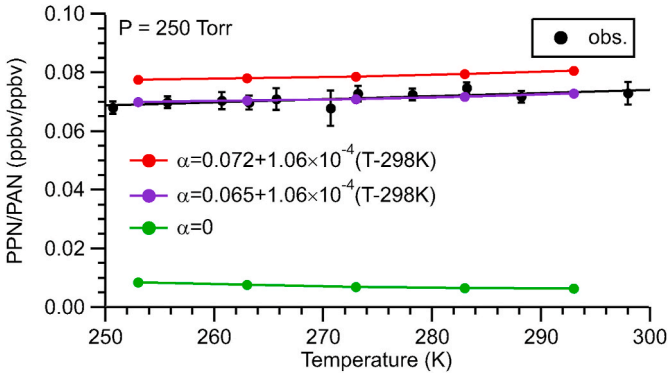

Fig. 3. Comparison of MCM box model simulations with experimental PPN:PAN ratios. See text for conditions of the simulations.

with those obtained with 285 nm UV-LEDs. Example chromatograms are shown in Fig. 4.

The ratios of peak areas (±1σ and uncorrected for the lower PPN sensitivity) were (6.83 ± 0.13) × 10^{-2} (N = 12) at 285 nm and (6.87 ± 0.28) × 10^{-2} (N = 12) at 315 nm and thus identical (t = 0.48 < 2.12). Hence, the observations at 285 nm are atmospherically relevant.

3.4. PPN:PAN ratios in the presence of an OH quencher

The MCM does not currently include R2b and R3b, i.e., OH production from reaction of acyl radicals with O_2. In the simulations, OH is produced from reaction between HO_2 and NO and appears as a side product in peroxy radical – peroxy radical reactions. If R2b and R3b were included, a larger fraction of PPN would have been predicted by the simulations.

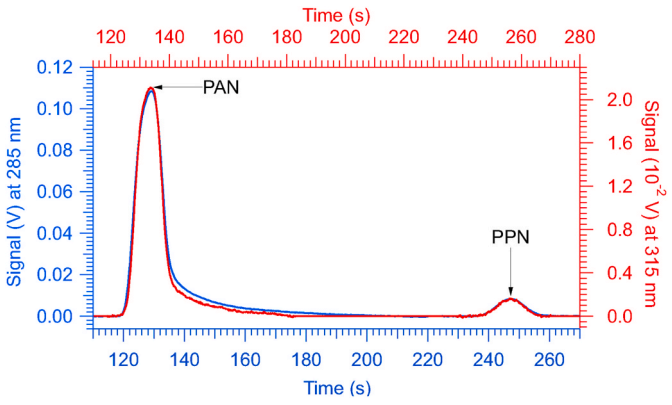

Fig. 4. Chromatogram of PPN:PAN ratios from irradiation of MEK in the presence of NO and O_2 at 285 nm (blue color, left and bottom axis) and at 315 nm (red color, top and right axis) at room temperature and atmospheric pressure. (For interpretation of the references to color in this figure legend, the reader is referred to the Web version of this article.)

Because a higher concentration of NO (which acts as sink of peroxy radicals) was used in the OH quenching experiment, PAN and PPN production was limited by radical production, i.e., by MEK photolysis. This was evident, for example, from absolute PAN and PPN concentrations that fluctuated on a time scale of 15–30 min, which were rationalized by fluctuations in the amount of MEK delivered from the glass trap on that time scale. Because of this, more NO_2 was available to react in secondary reactions that produce PAN or PPN. Furthermore, the PPN:PAN ratio (Fig. 5) took a considerable amount of time to stabilize. After several hours, the PPN:PAN ratio stabilized at (15 ± 2)% (1σ). The long stabilization period suggests that there was some accumulation or build-up of secondary species that ultimately raised the PPN:PAN product ratio.

When C_2H_6 was added to quench OH initiated chemistry, a PPN:PAN ratio of (7.4 ± 0.4)% (1σ) was observed after stabilization (Fig. 5), which is consistent with the earlier results (e.g., Fig. 1). The results obtained under NO_x-limited conditions presented earlier were likely more accurate because less OH is produced from reaction of HO_2 with NO, and the relatively stable and unreactive end products (i.e., PAN and PPN) are formed more quickly, thus reducing the effects of secondary chemistry. To err on the side of caution, the results under NO_x-limited conditions were pooled with those conducted in the presence of ethane to give a conservative value of α = (7 ± 1)% (2σ) at room temperature.

3.5. Comparison with literature and pressure dependence of α

The branching ratio observed in this work at 298 K, (7 ± 1)%, falls within the range of 6%–12% reported by Raber and Moortgart (1995), who had also used PAN and PPN to estimate α. However, the experiments described in this manuscript are more accurate and precise because they were conducted at lower concentration levels and were hence less affected by secondary chemistry. Furthermore, we used a calibrated GC for PAN and PPN determination (whereas Raber and Moortgart only estimated their sensitivity to PPN) and a narrower wavelength range for MEK photolysis.

Raber and Moortgart (1995) reported "effective" pressure dependent MEK quantum yields, mechanistically interpreted as a competition between dissociation of excited state MEK* and its collision-induced de-excitation. Based on their mechanism, α is not expected to be

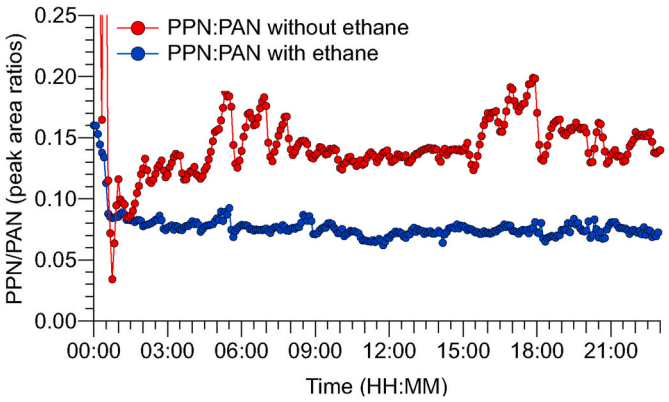

Fig. 5. Time series of PPN:PAN ratios from irradiation of MEK in the presence of NO and O_2 at 285 nm at room temperature and atmospheric pressure in the absence (data points shown in red color) and presence of ethane (data points shown in blue color). The addition of ethane prevents PPN formation via OH-initiated chemistry. (For interpretation of the references to color in this figure legend, the reader is referred to the Web version of this article.)

pressure dependent, consistent with what was observed in this work (Fig. 1). The pressure range investigated in this work covers conditions up to a height of ~10 km above sea level (COESA, 1976), which is where most MEK resides (Apel et al., 2003). At lower pressures, R2a and R3a may be sufficiently slow that R2b and R3b could become competitive, which could alter the PP:PA (and hence the PPN:PAN) ratio observed, though this is of little atmospheric interest.

Romero et al. (2005a; 2005b) and Khamaganov et al. (2007) irradiated MEK with 248 nm laser light but reported diverging α values of (19 ± 3)% and (0 ± 18)%, respectively. Our results are within the range reported by Romero et al. (2005a; 2005b) but are outside that reported by Khamaganov et al. (2007), though their error denotes 2σ precision and is not a full uncertainty. Khamaganov et al. (2007) noted that 248 nm light generates vibrationally excited $CH_3C(O)^*$ which is prone to dissociation forming CH_3 (quantified by absorption in their experiments). In contrast, vibrationally excited $C_2H_5C(O)^*$ is less prone to dissociation due to higher internal degrees of freedom. This led to a pronounced pressure-dependence and larger branching ratios in their experiments. Since the primary fragmentation branching ratio (α) was assumed to be independent of pressure (Khamaganov et al., 2007), the value that they ultimately reported was that of their highest-pressure experiment, which was least affected by dissociation but nevertheless should be viewed as an upper limit. In this work, a relatively long wavelength was used to irradiate MEK such that few, if any, vibrationally excited $CH_3C(O)^*$ molecules were generated, and this issue was avoided.

4. Conclusions

The MEK photolysis branching ratio at 285 nm was determined as $\alpha = (7 \pm 1)\% + (1.1 \pm 0.7) \times 10^{-4} \times (T\text{-}298)$ for 250 K < T < 300 K, where the uncertainties are at the 2σ level. The error bars in this expression do not include systematic uncertainties, such as errors in the relative sensitivity of PPN to PAN in the Varian PAN-GC (±4%), the potential error from the correction for OH initiated chemistry, and the relative rate coefficients of PA and PP radicals with other peroxy radicals (assumed to be equal).

Ketones such as MEK are important radical precursors in the troposphere, and the MCM is frequently used to model this radical chemistry in ambient air measurement campaigns (Edwards et al., 2014; Lu et al., 2013) and chamber studies (Fuchs et al., 2018). Current users of the MCM should examine and update the branching ratio parameterization for the MEK photolysis reaction. Those of other asymmetrically substituted ketones are likely also incorrectly parameterized in the MCM and should be investigated.

CRediT authorship contribution statement

Anna G. Zborowska: Investigation, Validation, Writing – review & editing. **Ceara Y. MacInnis:** Investigation, Formal analysis, Validation, Writing – review & editing. **Connie Z. Ye:** Investigation, Validation, Writing – review & editing. **Hans D. Osthoff:** Conceptualization, Funding acquisition, Methodology, Project administration, Resources, Software, Supervision, Writing – original draft, Writing – review & editing.

Declaration of competing interest

The authors declare that they have no known competing financial interests or personal relationships that could have appeared to influence the work reported in this paper.

Acknowledgments

This work was made possible by financial support from the Natural Sciences and Engineering Research Council of Canada (NSERC) in the form of a Discovery grant (RGPIN/03849-2016, to HDO). The authors thank Andrew Rickard and Mike Jenkin for personal communications.

References

Apel, E.C., Hills, A.J., Lueb, R., Zindel, S., Eisele, S., Riemer, D.D., 2003. A fast-GC/MS system to measure C2 to C4 carbonyls and methanol aboard aircraft. J. Geophys. Res.: Atmosphere 108, 8794. https://doi.org/10.1029/2002JD003199.

Atkinson, R., Baulch, D.L., Cox, R.A., Crowley, J.N., Hampson, R.F., Hynes, R.G., Jenkin, M.E., Rossi, M.J., Troe, J., 2006. Evaluated kinetic and photochemical data for atmospheric chemistry: volume II - gas phase reactions of organic species. Atmos. Chem. Phys. 6, 3625–4055. https://doi.org/10.5194/acp-6-3625-2006.

Brewer, J.F., Fischer, E.V., Commane, R., Wofsy, S.C., Daube, B.C., Apel, E.C., Hills, A.J., Hornbrook, R.S., Barletta, B., Meinardi, S., Blake, D.R., Ray, E.A., Ravishankara, A. R., 2020. Evidence for an oceanic source of methyl ethyl ketone to the atmosphere. Geophys. Res. Lett. 47 https://doi.org/10.1029/2019gl086045 e2019GL086045.

Brewer, J.F., Papanastasiou, D.K., Burkholder, J.B., Fischer, E.V., Ren, Y., Mellouki, A., Ravishankara, A.R., 2019. Atmospheric photolysis of methyl ethyl, diethyl, and propyl ethyl ketones: temperature-dependent UV absorption cross sections. J. Geophys. Res.: Atmosphere 124, 5906–5918. https://doi.org/10.1029/2019jd030391.

Burkholder, J.B., Sander, S.P., Abbatt, J.P.D., Barker, J.R., Huie, R.E., Kolb, C.E., Kurylo, M.J., Orkin, V.L., Wilmouth, D.M., Wine, P.H., 2015. Chemical Kinetics and Photochemical Data for Use in Atmospheric Studies, Evaluation Number 18. National Aeronautics and Space Administration. Jet Propulsion Laboratory, California Institute of Technology, Pasadena, California.

Coesa, 1976. U.S. Standard Atmosphere. In: Rumble, J.R. (Ed.), CRC Handbook of Chemistry and Physics, 101st ed. CRC Press, Boca Raton, FL. 1976.

Diau, E.W.G., Kötting, C., Zewail, A.H., 2001. Femtochemistry of norrish type-I reactions: I. Experimental and theoretical studies of acetone and related ketones on the S1 surface. ChemPhysChem 2, 273–293. https://doi.org/10.1002/1439-7641(20010518)2:5<273::aid-cphc273>3.0.co;2-h.

Edwards, P.M., Brown, S.S., Roberts, J.M., Ahmadov, R., Banta, R.M., deGouw, J.A., Dube, W.P., Field, R.A., Flynn, J.H., Gilman, J.B., Graus, M., Helmig, D., Koss, A., Langford, A.O., Lefer, B.L., Lerner, B.M., Li, R., Li, S.-M., McKeen, S.A., Murphy, S. M., Parrish, D.D., Senff, C.J., Soltis, J., Stutz, J., Sweeney, C., Thompson, C.R., Trainer, M.K., Tsai, C., Veres, P.R., Washenfelder, R.A., Warneke, C., Wild, R.J., Young, C.J., Yuan, B., Zamora, R., 2014. High winter ozone pollution from carbonyl photolysis in an oil and gas basin. Nature 514, 351–354. https://doi.org/10.1038/nature13767.

Edwards, P.M., Young, C.J., Aikin, K., deGouw, J., Dube, W.P., Geiger, F., Gilman, J., Helmig, D., Holloway, J.S., Kercher, J., Lerner, B., Martin, R., McLaren, R., Parrish, D.D., Peischl, J., Roberts, J.M., Ryerson, T.B., Thornton, J., Warneke, C., Williams, E.J., Brown, S.S., 2013. Ozone photochemistry in an oil and natural gas extraction region during winter: simulations of a snow-free season in the Uintah Basin, Utah. Atmos. Chem. Phys. 13, 8955–8971. https://doi.org/10.5194/acp-13-8955-2013.

Fuchs, H., Albrecht, S., Acir, I.H., Bohn, B., Breitenlechner, M., Dorn, H.P., Gkatzelis, G.I., Hofzumahaus, A., Holland, F., Kaminski, M., Keutsch, F.N., Novelli, A., Reimer, D., Rohrer, F., Tillmann, R., Vereecken, L., Wegener, R., Zaytsev, A., Kiendler-Scharr, A., Wahner, A., 2018. Investigation of the oxidation of methyl vinyl ketone (MVK) by OH radicals in the atmospheric simulation chamber SAPHIR. Atmos. Chem. Phys. 18, 8001–8016. https://doi.org/10.5194/acp-18-8001-2018.

Furgeson, A., Mielke, L.H., Paul, D., Osthoff, H.D., 2011. A photochemical source of peroxypropionic and peroxyisobutanoic nitric anhydride. Atmos. Environ. 45, 5025–5032. https://doi.org/10.1016/j.atmosenv.2011.03.072.

Hornbrook, R.S., Blake, D.R., Diskin, G.S., Fried, A., Fuelberg, H.E., Meinardi, S., Mikoviny, T., Richter, D., Sachse, G.W., Vay, S.A., Walega, J., Weibring, P., Weinheimer, A.J., Wiedinmyer, C., Wisthaler, A., Hills, A., Riemer, D.D., Apel, E.C., 2011. Observations of nonmethane organic compounds during ARCTAS Part 1: biomass burning emissions and plume enhancements. Atmos. Chem. Phys. 11, 11103–11130. https://doi.org/10.5194/acp-11-11103-2011.

Jenkin, M.E., Saunders, S.M., Pilling, M.J., 1997. The tropospheric degradation of volatile organic compounds: a protocol for mechanism development. Atmos. Environ. 31, 81–104. https://doi.org/10.1016/S1352-2310(96)00105-7.

Jenkin, M.E., Wyche, K.P., Evans, C.J., Carr, T., Monks, P.S., Alfarra, M.R., Barley, M.H., McFiggans, G.B., Young, J.C., Rickard, A.R., 2012. Development and chamber evaluation of the MCM v3.2 degradation scheme for β-caryophyllene. Atmos. Chem. Phys. 12, 5275–5308. https://doi.org/10.5194/acp-12-5275-2012.

Kabir, M., Jagiella, S., Zabel, F., 2014. Thermal stability of n-acyl peroxynitrates. Int. J. Chem. Kinet. 46, 462–469. https://doi.org/10.1002/kin.20862.

Kean, A.J., Grosjean, E., Grosjean, D., Harley, R.A., 2001. On-road measurement of carbonyls in California light-duty vehicle emissions. Environ. Sci. Technol. 35, 4198–4204. https://doi.org/10.1021/es010814v.

Khamaganov, V., Karunanandan, R., Rodriguez, A., Crowley, J.N., 2007. Photolysis of $CH_3C(O)CH_3$ (248 nm, 266 nm), $CH_3C(O)C_2H_5$ (248 nm) and $CH_3C(O)Br$ (248 nm): pressure dependent quantum yields of CH_3 formation. Phys. Chem. Chem. Phys. 9, 4098–4113. https://doi.org/10.1039/b701382e.

Le Crane, J.-P., Villenave, E., Hurley, M.D., Wallington, T.J., Ball, J.C., 2005. Atmospheric chemistry of propionaldehyde:kinetics and mechanisms of reactions with OH radicals and Cl atoms, UV spectrum, and self-reaction kinetics of $CH_3CH_2C(O)O_2$ radicals at 298 K. J. Phys. Chem. 109, 11837–11850. https://doi.org/10.1021/jp0519868.

Legreid, G., Lööv, J.B., Staehelin, J., Hueglin, C., Hill, M., Buchmann, B., Prevot, A.S.H., Reimann, S., 2007. Oxygenated volatile organic compounds (OVOCs) at an urban

background site in Zürich (Europe): seasonal variation and source allocation. Atmos. Environ. 41, 8409–8423. https://doi.org/10.1016/j.atmosenv.2007.07.026.

Lu, K.D., Hofzumahaus, A., Holland, F., Bohn, B., Brauers, T., Fuchs, H., Hu, M., Haseler, R., Kita, K., Kondo, Y., Li, X., Lou, S.R., Oebel, A., Shao, M., Zeng, L.M., Wahner, A., Zhu, T., Zhang, Y.H., Rohrer, F., 2013. Missing OH source in a suburban environment near Beijing: observed and modelled OH and HO_2 concentrations in summer 2006. Atmos. Chem. Phys. 13, 1057–1080. https://doi.org/10.5194/acp-13-1057-2013.

Martinez, R.D., Buitrago, A.A., Howell, N.W., Hearn, C.H., Joens, J.A., 1992. The near-UV absorption spectra of several aliphatic aldehydes and ketones at 300 K. Atmos. Environ. Part A-General Topics 26, 785–792. https://doi.org/10.1016/0960-1686(92)90238-G.

Nádasdi, R., Zügner, G.L., Farkas, M., Dóbé, S., Maeda, S., Morokuma, K., 2010. Photochemistry of methyl ethyl ketone: quantum yields and S1/S0-diradical mechanism of photodissociation. ChemPhysChem 11, 3883–3895. https://doi.org/10.1002/cphc.201000522.

Papadimitriou, V.C., Karafas, E.S., Gierczak, T., Burkholder, J.B., 2015. $CH_3CO + O_2 + M$ ($M = He, N_2$) reaction rate coefficient measurements and implications for the OH radical product yield. J. Phys. Chem. 119, 7481–7497. https://doi.org/10.1021/acs.jpca.5b00762.

Pitts, J.N., Blacet, F.E., 1950. Methyl ethyl ketone photochemical processes. J. Am. Chem. Soc. 72, 2810–2811. https://doi.org/10.1021/ja01162a544.

Raber, W.H., Moortgat, G.K., 1995. Photooxidation of Selected Carbonyl Compounds in Air: Methyl Ethyl Ketone, Methyl Vinyl Ketone, Methacrolein and Methylglyoxal. In: Barker, J. (Ed.), Progress and Problems in Atmospheric Chemistry. World Scientific Publishing Singapore.

Rajakumar, B., Gierczak, T., Flad, J.F., Ravishankara, A.R., Burkholder, J.B., 2008. The CH_3CO quantum yield in the 248 nm photolysis of acetone, methyl ethyl ketone, and biacetyl. Journal of Photochemistry and Photobiology A - Chemistry 199, 336–344. https://doi.org/10.1016/j.jphotochem.2008.06.015.

Rider, N.D., Taha, Y.M., Odame Ankrah, C.A., Huo, J.A., Tokarek, T.W., Cairns, E., Moussa, S.G., Liggio, J., Osthoff, H.D., 2015. Efficient photochemical generation of peroxycarboxylic nitric anhydrides with ultraviolet light-emitting diodes. Atmos. Meas. Tech. 8, 2737–2748. https://doi.org/10.5194/amt-8-2737-2015.

Roberts, J.M., Williams, J., Baumann, K., Buhr, M.P., Goldan, P.D., Holloway, J., Hubler, G., Kuster, W.C., McKeen, S.A., Ryerson, T.B., Trainer, M., Williams, E.J., Fehsenfeld, F.C., Bertman, S.B., Nouaime, G., Seaver, C., Grodzinsky, G., Rodgers, M., Young, V.L., 1998. Measurements of PAN, PPN, and MPAN made during the 1994 and 1995 nashville intensives of the southern oxidant study: implications for regional ozone production from biogenic hydrocarbons. J. Geophys. Res. 103, 22473–22490. https://doi.org/10.1029/98JD01637.

Romero, M.T.B., Blitz, M.A., Heard, D.E., Pilling, M.J., Price, B., Seakins, P.W., 2005a. OH formation from the $C_2H_5CO+O_2$ reaction: an experimental marker for the propionyl radical. Chem. Phys. Lett. 408, 232–236. https://doi.org/10.1016/j.cplett.2005.04.018.

Romero, M.T.B., Blitz, M.A., Heard, D.E., Pilling, M.J., Price, B., Seakins, P.W., Wang, L., 2005b. Photolysis of methylethyl, diethyl and methylvinyl ketones and their role in the atmospheric HO budget. Faraday Discuss 130, 73–88. https://doi.org/10.1039/b419160a.

Saunders, S.M., Jenkin, M.E., Derwent, R.G., Pilling, M.J., 2003. Protocol for the development of the Master Chemical Mechanism, MCM v3 (Part A): tropospheric degradation of non-aromatic volatile organic compounds. Atmos. Chem. Phys. 3, 161–180. https://doi.org/10.5194/acp-3-161-2003.

Sølling, T.I., Diau, E.W.G., Kötting, C., De Feyter, S., Zewail, A.H., 2002. Femtochemistry of norrish type-I reactions: IV. Highly excited ketones—experimental. ChemPhysChem 3, 79–97. https://doi.org/10.1002/1439-7641(20020118)3:1<79::aid-cphc79>3.0.co;2-#.

Sommariva, R., Cox, S., Martin, C., Borońska, K., Young, J., Jimack, P.K., Pilling, M.J., Matthaios, V.N., Nelson, B.S., Newland, M.J., Panagi, M., Bloss, W.J., Monks, P.S., Rickard, A.R., 2020. AtChem (version 1), an open-source box model for the Master Chemical Mechanism. Geosci. Model Dev. (GMD) 13, 169–183. https://doi.org/10.5194/gmd-13-169-2020.

Sommariva, R., de Gouw, J.A., Trainer, M., Atlas, E., Goldan, P.D., Kuster, W.C., Warneke, C., Fehsenfeld, F.C., 2011. Emissions and photochemistry of oxygenated VOCs in urban plumes in the Northeastern United States. Atmos. Chem. Phys. 11, 7081–7096. https://doi.org/10.5194/acp-11-7081-2011.

Tokarek, T.W., Huo, J.A., Odame-Ankrah, C.A., Hammoud, D., Taha, Y.M., Osthoff, H.D., 2014. A gas chromatograph for quantification of peroxycarboxylic nitric anhydrides calibrated by thermal dissociation cavity ring-down spectroscopy. Atmos. Meas. Tech. 7, 3263–3283. https://doi.org/10.5194/amt-7-3263-2014.

Villenave, E., Lesclaux, R., Seefeld, S., Stockwell, W.R., 1998. Kinetics and atmospheric implications of peroxy radical cross reactions involving the $CH_3C(O)O_2$ radical. J. Geophys. Res. 103, 25273–25285. https://doi.org/10.1029/98JD00926.

Wallington, T.J., Kurylo, M.J., 1987. Flash photolysis resonance fluorescence investigation of the gas-phase reactions of hydroxyl radicals with a series of aliphatic ketones over the temperature range 240-440 K. J. Phys. Chem. 91, 5050–5054. https://doi.org/10.1021/j100303a033.

Yáñez-Serrano, A.M., Nölscher, A.C., Bourtsoukidis, E., Derstroff, B., Zannoni, N., Gros, V., Lanza, M., Brito, J., Noe, S.M., House, E., Hewitt, C.N., Langford, B., Nemitz, E., Behrendt, T., Williams, J., Artaxo, P., Andreae, M.O., Kesselmeier, J., 2016. Atmospheric mixing ratios of methyl ethyl ketone (2-butanone) in tropical, boreal, temperate and marine environments. Atmos. Chem. Phys. 16, 10965–10984. https://doi.org/10.5194/acp-16-10965-2016.

Yujing, M., Mellouki, A., 2000. The near-UV absorption cross sections for several ketones. J. Photochem. Photobiol. Chem. 134, 31–36. https://doi.org/10.1016/S1010-6030(00)00243-4.

Zhang, G., Mu, Y.J., Zhou, L.X., Zhang, C.L., Zhang, Y.Y., Liu, J.F., Fang, S.X., Yao, B., 2015. Summertime distributions of peroxyacetyl nitrate (PAN) and peroxypropionyl nitrate (PPN) in Beijing: understanding the sources and major sink of PAN. Atmos. Environ. 103, 289–296. https://doi.org/10.1016/j.atmosenv.2014.12.035.

Zügner, G.L., Szilágyi, I., Zádor, J., Szabó, E., Dóbé, S., Song, X., Wang, B., 2010. OH yields for $C_2H_5CO+O_2$ at low pressure: experiment and theory. Chem. Phys. Lett. 495, 179–181. https://doi.org/10.1016/j.cplett.2010.06.089.